PAPER

A method for controlled growth of large MIL-88A crystals†

Erik Schumann, [iD] [a] Bianca Störr,[a] Uwe Böhme, [iD] [b]
Dominic Walter[a] and Florian Mertens [iD] *[a]

The most challenging aspect of the structural elucidation of novel metal–organic frameworks (MOFs) is presumably the small crystal size of the obtained compounds, since nanocrystallites cannot be analysed by X-ray single crystal diffraction without special equipment. In this paper, we present a new method based on the example of the well-known MIL-88A with which the size of the MOF crystals can be significantly increased by varying the reactants. It was shown that by replacing the originally used fumaric acid with fumaric acid esters, the fumarate ions are successively added to the reaction mixture because of the required ester hydrolysis, which results in a controlled growth of large MIL-88A crystals. In addition to the previously existing Rietveld refinements, it was thereby possible to obtain the first single crystal structure analysis of MIL-88A. This new method for growing large MOF crystals may thus provide access to the structural elucidation of further MOFs and offers a field of applications, such as the investigation of chemical reactions on defined MOF crystal surfaces.

1 Introduction

Since the first publication of the iron-containing isoreticular metal–organic framework MIL-88A in 2004,[1] several data on the synthesis, properties and application areas of this compound has been published.[2–5] The original synthesis route was based on the chemically controlled SBU approach, in which the SBU iron(III) acetate, fumaric acid and sodium hydroxide were reacted in water and methanol.[1,6,7] In later works, iron(III) chloride was used as reactant and water was used as the only solvent in hydrothermal syntheses.[8–11] Other solvents such as DMF were also utilised in some cases, which has, for instance, a substantial effect on the crystallite shape.[8,12,13] The structural investigations consisting of Rietveld refinements[14,15] based on powder XRD data showed the linking of trinuclear $\{Fe_3(\mu_3\text{-}O)\}^{7+}$ units by bidentate fumarate anions. One coordination site per iron(III) ion is occupied by a neutral ligand, such as water or methanol, so that the metal atoms are arranged in octahedral ligand spheres. This type of complex unit is singly positively charged, so that acetate ions are also in the structures to ensure electroneutrality. The comparatively simple synthesis procedure,

the inexpensive materials as well as the insensitivity to oxygen and humidity generated a high level of interest in this metal–organic framework. In most publications on potential applications, MIL-88A has been used as a catalyst for a wide variety of processes.[9,12,16–18] Further research has shown that this compound can also be used for arsenic removal in aqueous media[19] or for enzyme immobilisation.[20] However, the synthesis of MIL-88A from iron(III) compounds and fumaric acid provides crystallites of only a few micrometers[8,9,11,18–21] or even in the nanometer range,[10,16,12,17] independent of solvent and pH value. In this work we present a method for growing MIL-88A crystals of up to 250 μm, so that even a single crystal structure analysis could be carried out for the first time. As can be seen in Scheme 1, although an aqueous iron(III) chloride solution was taken for each of the different syntheses, corresponding esters were also used in addition to fumaric acid. The obtained MIL-88A samples were labelled according to the substituent of the respective fumaric acid esters. The following sections show that the modified synthesis route not only has an effect on the crystallite size, but also on the molecular structure and shape of the crystals.

2 Experimental section

2.1 Materials

Iron(III) chloride hexahydrate ($FeCl_3\cdot6H_2O$, ≥98%, Carl Roth), fumaric acid ($C_4H_4O_4$, 99%, Alfa Aesar), dimethyl fumarate ($C_6H_8O_4$, 99%, Thermo Fisher Scientific), diethyl fumarate ($C_8H_{12}O_4$, 98%, Thermo Fisher Scientific), methanol (CH_4O, ≥99.8%, VWR), ethanol (C_2H_6O, ≥99.9%, Sigma-Aldrich),

[a] TU Bergakademie Freiberg, Fakultät für Chemie, Physik und Biowissenschaften, Institut für Physikalische Chemie, Leipziger Str. 29/Lessingstr. 45, D-09599 Freiberg, Germany. E-mail: Florian.Mertens@chemie.tu-freiberg.de
[b] TU Bergakademie Freiberg, Fakultät für Chemie, Physik und Biowissenschaften, Institut für Anorganische Chemie, Leipziger Str. 29, D-09599 Freiberg, Germany
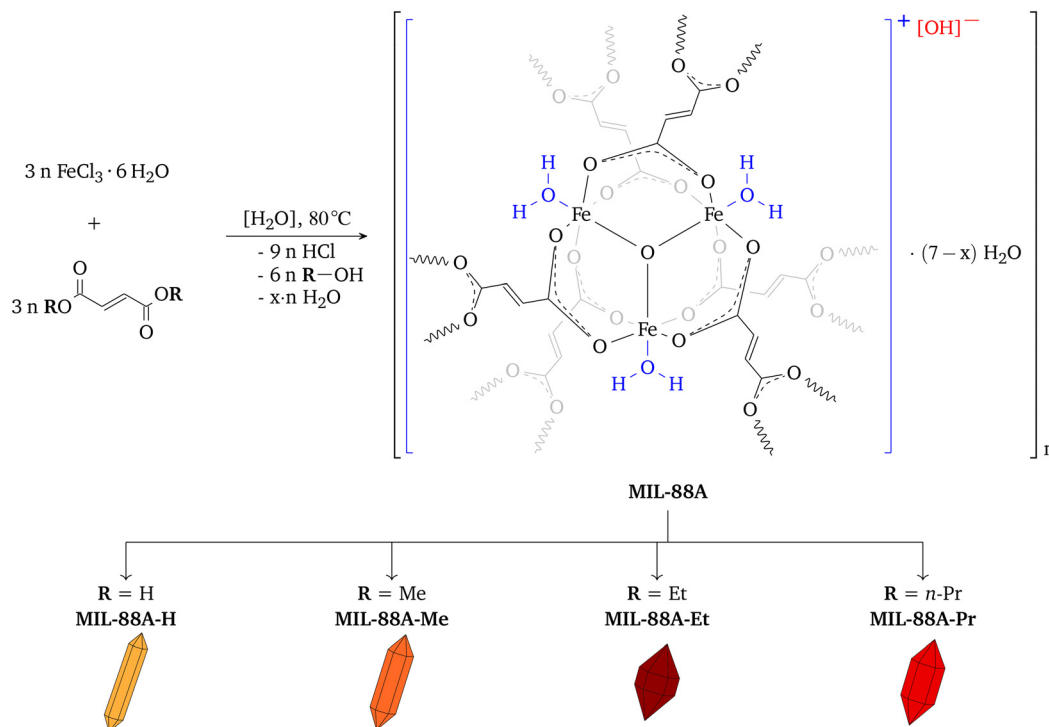
Scheme 1 General reaction equation for the synthesis of MIL-88A; labelling of the obtained MIL-88A samples according to the groups on the different fumaric acid derivatives used; illustration of the corresponding crystal shapes.

1-propanol (C_3H_8O, 99.8%, VWR), sulfuric acid (H_2SO_4, >95%, Fisher Scientific), toluene (C_7H_8, technical grade), sodium bicarbonate ($NaHCO_3$, 99%, Sigma-Aldrich), diethyl ether ($C_{43}H_{10}O$, technical grade), sodium chloride (NaCl, technical grade), anhydrous sodium sulfate (Na_2SO_4, ≥99.5%, Fisher Scientific) and deuterated dimethyl sulfoxide (C_2D_6OS, 99.8%, DEUTERO) were used as received.

2.2 Characterisation techniques

PXRD. Diffractograms were acquired with a Bruker D2 PHASER diffractometer using Cu-K_α radiation ($\lambda = 1.54184$ Å). The angles are given in ° 2θ. The samples were prepared on a stainless steel sample holder and sealed with a plastic dome. To ensure that the fully hydrated forms of the MOF samples were characterised, suspensions in deionised water were measured. The relative intensities of the reflections are given in brackets.

Crystal structure determination. Single crystal X-ray diffraction data were obtained from crystals of sample **MIL-88A-Et** with a STOE IPDS-II image plate diffractometer equipped with a low-temperature device with Mo-K_α radiation ($\lambda = 0.71073$ Å) using ω and ϕ scans. The sample consists of only very small crystals. The crystal under investigation had a size of $0.15 \times 0.2 \times 0.2$ mm^3 and was extreme weakly diffracting. Scan times of 12 minutes per frame were applied and resulted in a useable data set. Crystal data and details of structure refinement are summarised in Table 1. The software X-AREA was used for data collection and cell refinement and X-RED for data reduction.[22]

Structure solutions were performed with direct methods[23] and the structures were refined by full-matrix least-squares

Table 1 Data of crystal, data collection and structure refinement for compound **MIL-88A-Et**

Compound	MIL-88A-Et
Empirical formula	$Fe_3C_{12}H_{12}O_{16}$
Formula weight	579.77
T, K	153
λ, Å	0.71073
Crystal system	Hexagonal
Space group	$P6_3/m$
a, Å	13.6085(4)
b, Å	13.6085(4)
c, Å	12.7623(5)
α, °	90
β, °	90
γ, °	120
Z/Dc, g cm^{-3}	2/0.941
μ, mm^{-1}	1.0882
$F(000)$	580
Crystal size, mm	$0.15 \times 0.2 \times 0.2$
θ range for data coll.	2.352–28.092
Reflections collected	29813
Indep. refl./R(int)	1736/0.0902
Completen. to θ_{max}	99.9%
Refinement method	Full-matrix least-squares on F^2
Data/restraints/param.	1736/3/59
Goodness-of-fit on F^2	1.064
R_1/wR_2 [$I > 2\sigma(I)$]	0.0683/0.2190
R_1/wR_2 (all data)	0.0737/0.2242
L. diff. peak/hole, e Å^{-3}	0.899/−0.817

calculations based on F^2 for all reflections using SHELXL.[24] Hydrogen atoms were included in the models in calculated positions and were refined as constrained to the bonding atoms. Solution and refinement were performed in the hexagonal space group $P6_3/m$. Furthermore, the investigated crystal was a twin with a twofold axis, which was incorporated in the refinement. Six oxygen atoms, which belong to water molecules, were located in the asymmetric unit during refinement. It was not possible to locate or refine any corresponding hydrogen atoms. Therefore, these oxygen atoms were squeezed from the structure model (SQUEEZE procedure from PLATON[25]) and the final refinement was performed without solvent water. 484 electrons in the solvent accessible volume of 1272 Å^3 were found in the unit cell. Fig. S1 (see ESI†) contains a selection of atomic distances and angles. CCDC-2427039 contains the supplementary crystallographic data for this paper.

Optical microscopy. A Zeiss Stemi 2000-C microscope was used to obtain the light microscopy images. The microscope was equipped with an ScopeTek DCM-310 camera. The ScopePhoto (version ×86, 3.1.268) software was used to capture the frames. The magnification can be seen in Fig. 1 by means of the illustrated scale.

TG-DSC-FTIR. TG-DSC measurements were carried out on a Sensys TG-DSC (SETARAM). 5 mg of the compounds were weighed into a corundum crucible inside the glove box. The samples were heated to 600 °C with a constant heating rate of 5 K min^{-1} in a stream of argon at a flow rate of 20 cm^3 min^{-1}. The decomposition gases were identified by means of an FTIR spectrometer (Varian 3100 FTIR, Excalibur Series) at the purge gas outlet.

NMR. ^{1}H (500.13 MHz) and ^{13}C (125.76 MHz) NMR data were obtained on a Bruker Avance III 500 MHz spectrometer. The samples were prepared by dissolving 30 mg sample in 0.5 mL of DMSO-d$_6$. The chemical shifts of the ^{1}H and ^{13}C NMR spectra are given in ppm relative to SiMe$_4$ (internal standard). NMR data were processed by using the Bruker TopSpin 4.0.7 software.

Sorption isotherms. BET measurements were recorded with a BELSORP-mini II (BEL JAPAN, INC). A BET tube was filled with 80 mg of material using a long-neck funnel. The tube was equipped with a suitable glass rod to reduce the dead volume and closed with a valve suitable for working under air exclusion. The samples were pretreated at 125 °C under reduced pressure over night. Dead volume correction

was done with helium in an empty BET tube with a glass rod of approximately the same size. The sorption measurements were carried out with nitrogen. The adsorption curve was measured up to a relative pressure of 0.995 and the subsequent desorption curve down to a relative pressure of 0.05. The sorption measurements and the determination of the specific surface area were carried out four times.
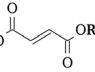
Hydrolysis kinetics using GC-FID. The reaction mixtures for investigation of hydrolysis kinetics of the fumaric acid esters were analysed quantitatively with a GC-FID (HP 5890 Series II, headspace sampler: HP 7694, column: HP-1). The GC-FID was calibrated for the hydrolysis products methanol, ethanol and 1-propanol by concentration-dependent measurements of aqueous solutions in 20 cm^3 GC headspace vials (see ESI† Fig. S13–S15). A pH = 1 sulphuric acid was used as solvent for the hydrolysis experiments by diluting 2.564 g of a 96% sulphuric acid with distilled water in a 500 cm^3 volumetric flask. The hydrolysis experiments were carried out in 20 cm^3 GC headspace vials. For each experiment, 4 mmol of the corresponding fumaric acid ester were mixed with 2.000 g of the diluted sulphuric acid. The vial was sealed and placed in a drying oven at 80 °C. After a defined reaction time, the vial was removed and measured using GC-FID. The amount of produced alcohol was used to calculate the amount of the remaining ester.

Calculation of the surface area. The theoretical surface area of **MIL-88A-Et** was calculated by means of the Mercury[26] tool void (contact surface method) using a probe radius of 2 Å and grid spacing of 0.2 Å. Data set CCDC-2427039 was used, in which the solvent water molecules inside of the pores have already been removed by applying the SQUEEZE procedure from PLATON.[25]

2.3 Synthetic procedures

Preparation of MIL-88A. In a 50 cm^3 SCHOTT bottle, 1.622 g of FeCl$_3$·6H$_2$O (6 mmol) were dissolved in 30 cm^3 of distilled water. Equimolar amounts of the respective fumaric acid derivatives (6 mmol each) were added. The SCHOTT bottle was sealed and placed in a drying oven at 80 °C without a stirrer. The exact weights, yields and reaction times can be found in Table 2. The obtained crystals were filtered, washed thoroughly with distilled water and dried overnight at room temperature and ambient pressure. XRD. **MIL-88A-H** 7.4 (1.00), 8.3 (0.04), 10.1 (0.31), 20.4 (0.05), 22.2 (0.37), 24.1

Table 2 Overview of the masses of the different fumaric acid derivatives used, the reaction times and the yields of the syntheses

Compound	mass of RO—(fumarate)—OR		Reaction time	Yield
MIL-88A-H	R = H	0.696 g	24 h	0.660 g
MIL-88A-Me	R = Me	0.865 g	72 h	0.626 g
MIL-88A-Et	R = Et	1.033 g	7 days	0.634 g
MIL-88A-Pr	R = n-Pr	1.201 g	28 days	0.323 g

(0.05), 27.7 (0.07), 28.9 (0.08), 29.7 (0.09), 30.7 (0.10); **MIL-88A-Me** 7.4 (1.00), 10.1 (0.58), 12.8 (0.08), 13.9 (0.06), 19.0 (0.04), 20.4 (0.11), 22.2 (0.50), 24.1 (0.05), 27.7 (0.06), 28.9 (0.08), 29.7 (0.12), 30.7 (0.18); **MIL-88A-Et** 7.4 (0.34), 10.1 (1.00), 12.8 (0.64), 13.9 (0.65), 15.7 (0.22), 19.0 (0.26), 20.4 (0.33), 22.2 (0.36), 24.1 (0.32), 27.7 (0.40), 28.9 (0.37), 29.4 (0.32), 30.7 (0.60), 32.5 (0.31); **MIL-88A-Pr** 7.4 (0.95), 10.1 (1.00), 12.8 (0.14), 13.9 (0.08), 20.4 (0.16), 22.2 (0.33), 24.1 (0.10), 27.7 (0.10), 28.9 (0.09), 29.7 (0.10), 30.7 (0.14).

Preparation of dipropyl fumarate. In a 250 cm³ single-necked flask, 23.214 g of fumaric acid (200 mmol), 120 cm³ of 1-propanol (4-fold excess), 2 cm³ of concentrated sulfuric acid and 25 cm³ of toluene were refluxed for 12 h. The reaction mixture was poured onto 100 g of crushed ice. Sodium bicarbonate was added until no more gas evolution was observed. The mixture was transferred into a separatory funnel and extracted three times with 25 cm³ of diethyl ether. The organic phases were combined and washed in the separatory funnel with an aqueous solution of sodium chloride. The combined organic phase was dried over sodium sulfate and filtered. After separation of the solvents, the product was fractionally distilled (b.p.: 106 °C at 5 mbar). 23.770 g (59.4%) of dipropyl fumarate were obtained as a colourless liquid. NMR. δ_{1H} (ppm) = 6.77 (s, 2H, CH), 4.12 (t, $^3J_{H-H}$ = 7.1 Hz, 4H, O–CH₂), 1.65 (sex, 4H, $\underline{CH_2}$–CH₃), 0.91 (t, 6H, CH₃); δ_{13C} (ppm) = 164.8 (C=O), 133.6 (CH), 66.9 (O–CH₂), 21.8 ($\underline{CH_2}$–CH₃), 10.6 (CH₃).

3 Results and discussion

3.1 Synthesis of MIL-88A with fumaric acid esters

The attempts to improve the synthesis of MIL-88A in this paper were not performed using the chemically controlled SBU[1,6,7] method. Therefore, no iron(III) acetate was used as SBU, but iron(III) chloride was used as reactant. In order to reproduce the corresponding literature of this synthesis approach,[8,10,13] iron(III) chloride was reacted with fumaric acid, resulting in the formation of nanocrystalline **MIL-88A-H**. A reaction temperature of 80 °C was set for all experiments. Optical microscopy images, which can be found in Fig. 1(a), were taken to determine the size of the different crystallites. As was to be expected with the magnification used, the individual crystals in the powder are only barely recognisable. Fumaric acid is almost insoluble in water, so that at the start of the reaction a yellow solution with a white suspended solid was present. Observing the progress of the reaction was difficult because **MIL-88A-H** formed as a light-orange solid within 24 h.

We hypothesised that a slower supply of fumarate ions to the iron(III) ions would lead to a more controlled growth of
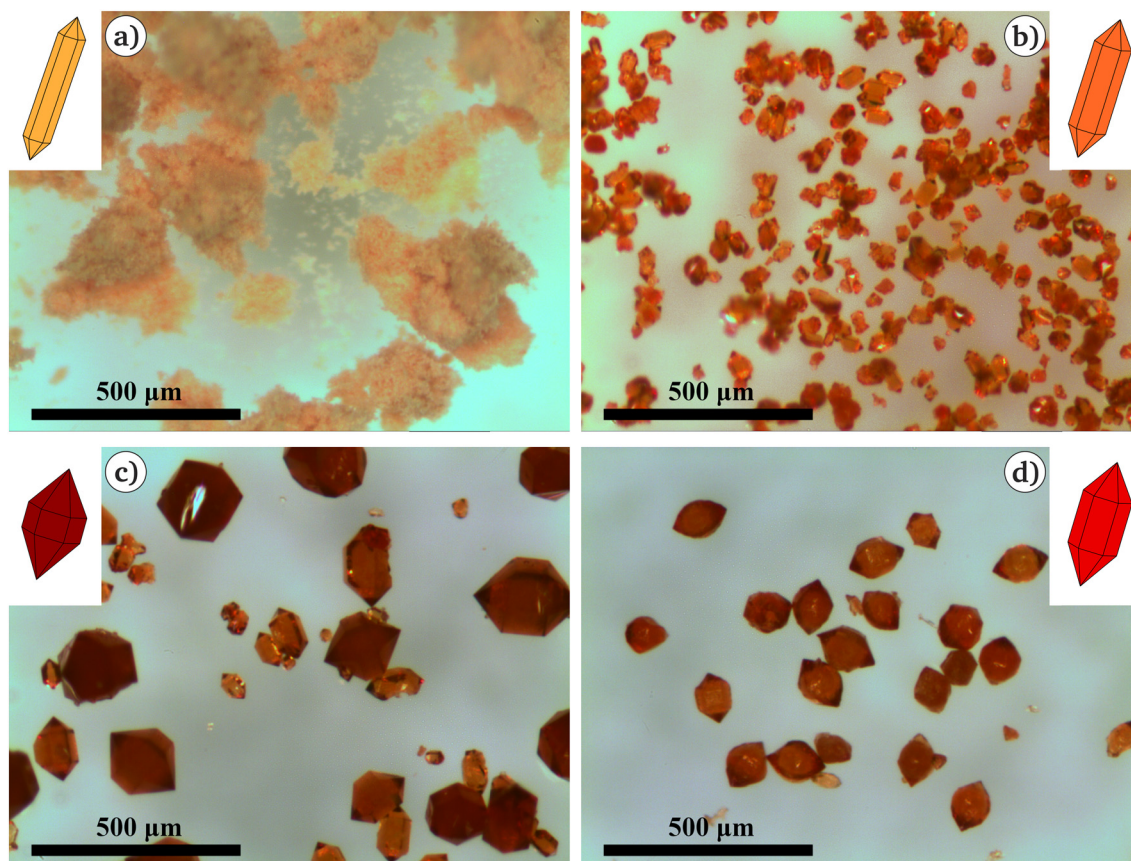

Fig. 1 Microscopy images of the MIL-88A samples; a) **MIL-88A-H**; b) **MIL-88A-Me**; c) **MIL-88A-Et**; d) **MIL-88A-Pr**; used magnification is represented by the black bar (500 μm).

the MOF crystals. The idea was therefore to use fumaric acid esters instead of fumaric acid. An iron(III) chloride solution has a low pH value which is sufficient for acidic ester hydrolysis. Thus, the ester bonds must first be cleaved before the resulting fumarate ions can form the MIL-88A network. When dimethyl fumarate was used as a reactant instead of fumaric acid, there were some significant differences. Dimethyl fumarate is also a white solid that is almost insoluble in water, so that a similar suspension was also present in this case. A yellow nanocrystalline precipitate also formed in this synthesis within 48 h. However, within the next 24 h, small red crystals grew from this sludge-like reaction mixture, which eventually accumulated at the bottom of the reaction bottle. As can be seen in Fig. 1(b), after an overall reaction time of 3 days, **MIL-88A-Me** was found as a red crystalline solid with a crystallite size of about 50 μm. The typical hexagonal crystal shape can already be recognised in the light microscopy image of this synthesis product.

Another significant increase in the size of the resulting crystals was achieved by using diethyl fumarate. As can be seen from Table 2, the reaction time of this synthesis was 7 days in total. Initially, there was also a difference in observing the progress of the reaction. In contrast to the previously used reactants, diethyl fumarate is a colourless, almost water-insoluble liquid that has a lower density than water. Accordingly, the compound accumulated as colourless pearls on the surface of the orange iron(III) chloride solution. Within 5 days, again an orange sludge-like mixture formed, from which crystals grew after two more days. However, the significant difference between the formed **MIL-88A-Et** crystals and the previous experiments was that their colour was dark red and the individual crystallites were already visible to the bare eye. The microscopy image (see Fig. 1(c)) confirmed this

impression, as the crystallite size was now up to 200 μm. From these results, we assumed that further elongation of the alkyl chain on the fumaric acid ester would not only increase the reaction time but also the crystallite size. Thus, dipropyl fumarate, which is also an almost water-insoluble liquid with a lower density than water, was used in another synthesis approach. However, we found that the first red crystals only grew out of the sludge after about 21 days and the reaction took another 7 days to complete. This resulted in a total time of 4 weeks and unfortunately no further enlargement of the crystallites. On the contrary, as can be seen in Fig. 1(d), the approximately 100 μm large **MIL-88A-Pr** crystals are even smaller than those of **MIL-88A-Et**. We suspect that this phenomenon is because of the low solubility of the reactant. Both the fumaric acid and the fumaric acid esters used are almost insoluble in water. This property is helpful for the course of the syntheses investigated here, as small amounts of reactant are gradually dissolved in the iron(III) chloride solution and the solid MOF crystals are slowly formed in this way. However, it seems that the solubility of dipropyl fumarate is even too low, so that not enough fumarate ions are available for the growth of the **MIL-88A-Pr** crystallites. Accordingly, under the applied synthesis conditions, the best results regarding the size of the crystals are achieved by using diethyl fumarate.

Fig. 1 shows that not only the size of the crystallites depends on the ester used, but also the morphology of the crystals. As can be seen in Fig. 2, the intensities of the reflections in the powder diffractograms represent the different crystal morphologies as a result of texture. In accordance with the literature,[18,27] the terms needle, rod, diamond and spindle are also used in this paper for the different morphologies. In the cited publications, however, the change in crystal shape was not caused by the use of different reactants, but by varying the
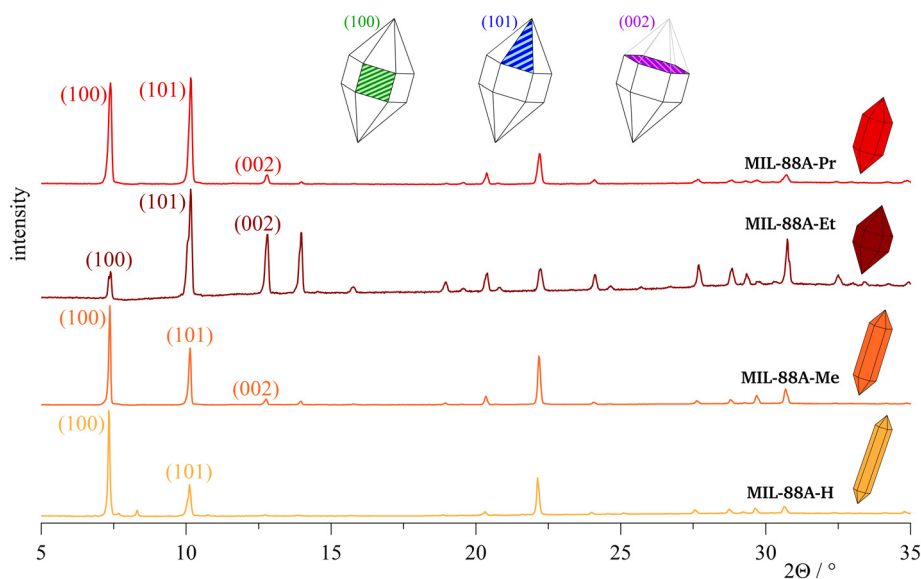

Fig. 2 Powder XRD patterns of the different MIL-88A-samples; indexing was adapted from the literature;[6,12] illustration of the reflection indices by the corresponding crystal planes.

solvent, the reaction temperature, the reactant ratios used or the reaction time. Nevertheless, the results show certain similarities to the data found here. The indexing of the reflections in the powder diffractograms was also done according to the literature.[6,12]

In the diffractogram of the **MIL-88A-H** sample (see Fig. 2), because of texture the (100) reflection is the most intense, (101) is clearly less intense and (002) is almost unrecognizable. This pattern corresponds to expectations, as **MIL-88A-H** consists of long, thin needles, which are statistically preferred lying on the side plane. In contrast, the reflections (101) and (002) of the rod-like crystals within sample **MIL-88A-Me** are more intense because the crystallites are thicker and shorter compared to **MIL-88A-H**. As a result, the probability that the crystallites in powder sample **MIL-88A-Me** lie on a plane at the crystal top is higher than for sample **MIL-88A-H**. If diethyl fumarate is used as the reactant, the resulting crystals of sample **MIL-88A-Et** have a diamond shape. The corresponding diffractogram shows that the (101) reflection is now the most intense and (002) also has a higher intensity than (100). The spindle-shaped crystals of the **MIL-88A-Pr** sample show approximately the same intensity for (100) and (101), from which it can be concluded that lying on a side plane has approximately the same probability as lying on a plane at the top of the crystal. We assume that the influence on the morphology of the crystallites is caused by the presence of the decomposition products of the used esters. Depending on which ester was taken as the reactant, methanol, ethanol or 1-propanol is generated during the reaction. In this way, the composition of the solvent changes during the course of the reaction. Accordingly, this effect is quite comparable with the observations in the literature, in which, for instance, a variation in the solvent ratio of water : DMF resulted in similar crystal shapes.

3.2 Single crystal structure analysis of MIL-88A-Et

Of all the crystal shapes obtained in this work, the diamond-like crystals are the most suitable ones for investigation using single crystal X-ray diffraction. As shown in Fig. 1, the diamond-shaped crystals of sample **MIL-88A-Et** were also the largest of all, with a size of up to 200 μm. Because of these characteristics, it was possible to perform a single crystal structure analysis of MIL-88A for the first time. As will be discussed in the following, our results are in good accordance with the two existing RIETVELD refinements in the literature.[14,15]

Fig. 3 shows the asymmetric unit of **MIL-88A-Et**. As already described in the experimental section, all solvent-water molecules were squeezed out from the structure before final refinement. The compound crystallises with a high symmetry in the space group $P6_3/m$. In the center of the structure is the μ_3 oxygen atom (O1), through which runs a 6-fold rotoinversion axis. Orthogonal to this axis is the trigonal $\{Fe_3(\mu_3\text{-}O)\}^{7+}$ plane after applying the symmetry elements.
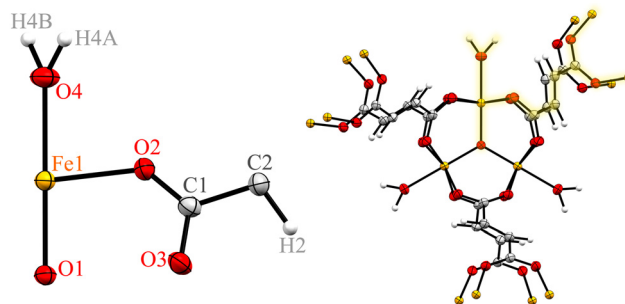

Fig. 3 Left: Asymmetric unit of **MIL-88A-Et** with labelling of the atoms; right: illustration of the secondary building unit including the fumarate anions and coloured highlighting of the asymmetric unit; thermal ellipsoids with 50% probability.

The three iron atoms of this central substructure are bridged by six fumarate ions (O2, O3, C1, C2). Coordinatively bound water molecules are located at the sixth coordination sites of the iron atoms, which results in all metals being located in octahedral ligand spheres.

The **MIL-88A-Et** crystals were obtained from an aqueous solution and were not dried prior to X-ray analysis. In order to better visualise the pore structure and the water contained in the pores, Fig. 4 shows a packing view of the crystal structure with water before the final refinement in comparison to the squeezed structure without water. In the initial refinement steps, the oxygen atoms of six solvent-water molecules were located in the asymmetric unit.

The distance between Fe1 and the central μ_3 oxygen atom O1 of 1.8925(9) Å is significantly shorter than between Fe1 and the fumarate oxygens O2 and O3 (2.004(4) Å). This difference is in line with the expectations and can be explained by the trinuclear character of the central substructure. Accordingly, the O–Fe–O angle between the μ_3-O atom and the fumarate oxygens (95.98(11)°) is also larger than between the water-oxygen atom and the fumarate oxygens (84.02(15)°). These data are in good match with those from the two Rietveld refinements.[14,15]

The decisive difference to the literature is the type of anion, which is necessary because of the electroneutrality as explained in Scheme 1. In the structures from literature, acetate ions are found as anions. Because of the use of iron(III) chloride as a reactant, we expected chloride ions to be present in our structure. However, no chlorine atoms were found within the X-ray analysis. For this reason, we assume that the ionic charge balance is achieved by a missing proton on one of the solvent water molecules. This hypothesis is visualised by the illustration in Fig. 5. Presumably, the hydrogen bond network of the pore water in the asymmetric unit does not contain six complete water molecules, but only five and one hydroxide ion. Unfortunately, the data set was too weak in terms of reflection intensities to locate the hydrogen atoms of the water network.

We carried out a series of experiments to remove the water from the pores and thereby activate the MOF. Unfortunately, we did not succeed in preserving the pore structure during activation, so that no single crystal structure analysis of the
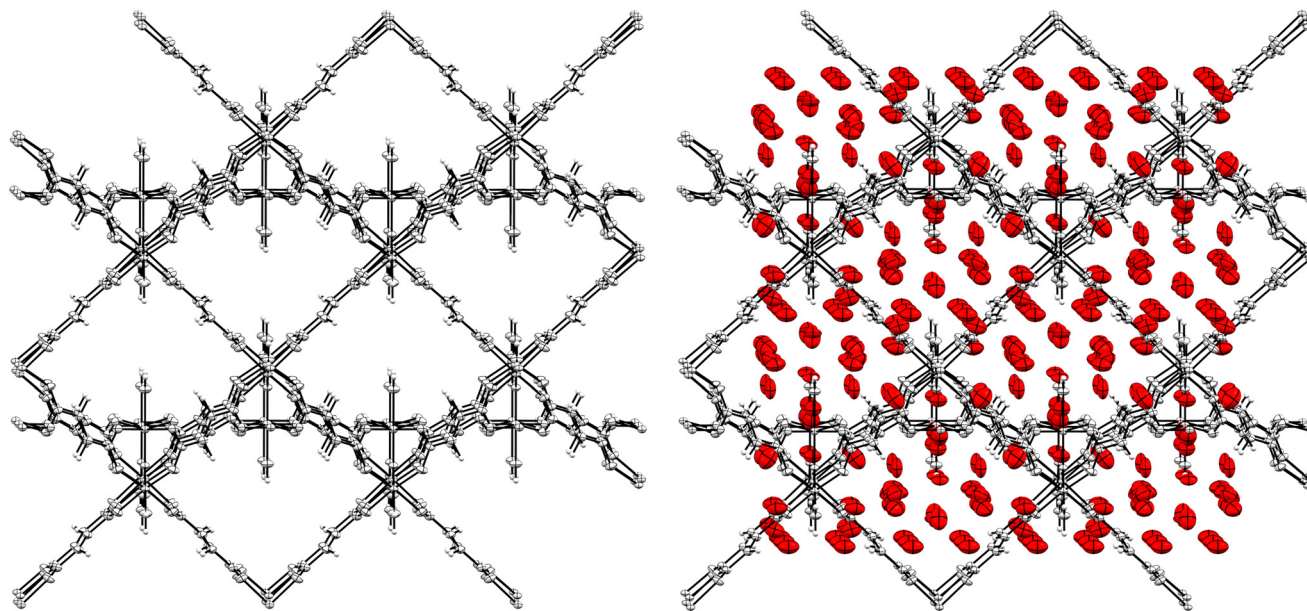
Fig. 4 Packing view of **MIL–88A-Et**, with secondary building unit and linker ions shown in gray colour; left: after final refinement without solvent water; right: before final refinement including solvent water (only the oxygen atoms in red colour); thermal ellipsoids with 50% probability.

anhydrous MIL-88A could be performed. Fig. S2 (see ESI†) shows as an example the highly fragmented crystals after activation. This phenomenon is also the reason why the specific BET surface areas of the samples are rather small and not as high as expected for typical metal–organic frameworks (see ESI† Fig. S3 and S4). The BET surface area of **MIL-88A-H** has a size of (110 ± 7) m^2 g^{-1}. This value is in good accordance to the literature, which gives data between 6.72 and 359 m^2 g^{-1}.[11,28,29] The surfaces of the other samples are too small to be meaningfully determined using the BET method.

The thermogravimetric analyses of the four MIL-88A samples show that the linker molecules are thermally decomposed at around 250 °C (see ESI† Fig. S5 and S8). This decomposition temperature is likewise verified by literature data.[10,13,17,30–32] Although, according to the analyses only water is measurable as a decomposition product at around 100 °C, we nevertheless presume that the framework is not

temperature-resistant and the pores collapse. However, the calculation of the total surface area of 1332 m^2 g^{-1} obtained from the single crystal structure analysis data of **MIL-88A-Et** shows that MIL-88A has a porous structure in principle. Details on the determination of the surface area are described in the experimental section and a graphical illustration of the calculated pores in data set CCDC-2427039 can be found in Fig. S12 (see ESI†). In the future, we will attempt to preserve the pore structure during activation in order to obtain a single crystal structure analysis of the activated sample and thus get more information about porous MIL-88A. These planned strategies include, for example, successive washing with solvents that have a gradually decreasing polarity and a lower boiling point than water. We also plan to replace the water in the pores with DMSO molecules. In this way, we hope to achieve a better characterisation of the pore structure using single crystal X-ray diffraction, as sulphur atoms are more readily measurable than oxygen atoms with this analysis technique. Furthermore, we will combine the exchange of the solvents with a particularly gentle way of removing the solvents by means of pressure and temperature gradients. The results generated in this context will be the focus of a future work.
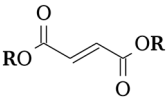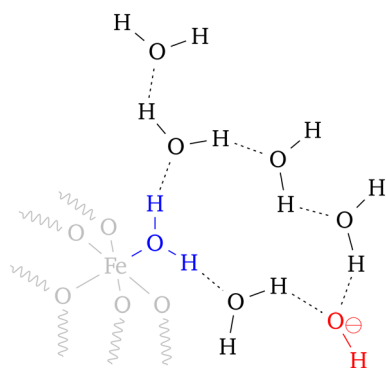
3.3 Hydrolysis kinetics of fumaric acid esters

In order to substantiate the results from section 3.1, the acidic hydrolysis of the different fumaric acid esters used was investigated quantitatively by means of GC-FID (headspace). Diluted sulphuric acid with a pH value of 1 was used for all experiments, further details can be found in the experimental section. The acidic cleavage of an ester (eqn (1)) proceeds according to second-order reaction kinetics with a reaction rate constant k (eqn (2)). Since water was used as a solvent

Fig. 5 Schematic illustration of a hydroxide ion as a counterion because of electroneutrality through the absence of a proton in a hydrogen bonding solvent water network.

Table 3 Determined reaction rate constants k' for the acid hydrolysis experiments of the different fumaric acid esters

	Rate constant k'/h^{-1}
R = Me	$(1.49 \pm 0.08) \times 10^{-1}$
R = Et	$(4.33 \pm 0.41) \times 10^{-2}$
R = n-Pr	$(3.14 \pm 0.09) \times 10^{-3}$

and is therefore present in high excess, its amount of substance n_{water} was assumed to be constant over time. Therefore, the kinetic experiments were evaluated by applying the pseudo-first-order rate eqn (5) with the reaction rate constant k'. The reverse reaction of eqn (1) in terms of the formation of the ester by a chemical equilibrium is neglected for the following considerations.
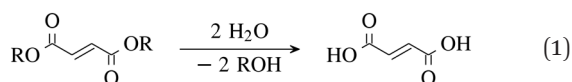
$$\frac{\text{d}n_{\text{ester}}}{\text{d}t} = -k \cdot n_{\text{ester}} \cdot n_{\text{water}}^2 \tag{2}$$

$$k' = k \cdot n_{\text{water}}^2 \tag{3}$$

$$\frac{c_{\text{ester}}}{\text{d}t} = -k' \cdot n_{\text{ester}} \tag{4}$$

$$ln\left(\frac{n_{\text{ester}}}{n_{\text{ester},0}}\right) = -k' \cdot t \tag{5}$$

The corresponding graph and the calculated k' values from the linear regressions can be found in Fig. S16 (see ESI†) as well as in Table 3. This illustration shows that the reaction rate of acidic ester cleavage decreases significantly as the alkyl group increases. These data support our hypothesis that the ester hydrolysis is the rate-determining step in the synthesis of MIL-88A and thus has a major influence on crystal growth.

4 Conclusions

In this work it was shown that small modifications of the reactants can be used to remarkably change the crystal size as well as the morphology of MIL-88A. The literature synthesis using iron(III) chloride and fumaric acid results in a nanocrystalline powder. However, if fumaric acid esters are used instead of fumaric acid, it not only has an effect on the crystal shape, but especially on the size of the crystallites. We attribute the influence of crystal growth to the solubility of the reactants on the one hand and the acidic hydrolysis required before the fumarate ions can function as linkers between the SBUs on the other. The larger the alkyl group on

the ester, the lower is the water solubility and the higher is the required reaction time. Contrary to expectations, the largest crystals were obtained in the case of diethyl fumarate, as dipropyl fumarate has such a low solubility that no controlled growth of large crystals was possible. If iron(III) chloride is reacted with diethyl fumarate, it was even possible for the first time to obtain a single-crystal structure analysis of MIL-88A with crystals up to 200 μm in size. The method discussed in this paper is a case study which can potentially be applied to other MOF systems.

Data availability

The data supporting this article have been included as part of the ESI.† Supplementary crystallographic data for **MIL-88A-Et** has been deposited at the CCDC under 2427039 and can be obtained from **https://www.ccdc.cam.ac.uk/**.

Author contributions

Conceptualisation, E. S., B. S.; methodology, E. S., B. S., D. W.; investigation, E. S., B. S., U. B., D. W.; resources, F. M.; writing – original draft, E. S.; writing – review & editing, E. S., B. S., U. B., D. W., F. M.; visualisation, E. S., U. B.; funding acquisition, F. M.

Conflicts of interest

There are no conflicts to declare.

Acknowledgements

References

1 C. Serre, F. Millange, S. Surblé and G. Férey, *Angew. Chem., Int. Ed.*, 2004, **43**, 6285–6289.

2 N. Stock and S. Biswas, *Chem. Rev.*, 2012, **112**, 933–969.

3 M. Rubio-Martinez, C. Avci-Camur, A. W. Thornton, I. Imaz, D. Maspoch and M. R. Hill, *Chem. Soc. Rev.*, 2017, **46**, 3453–3480.

4 M. Ding, X. Cai and H.-L. Jiang, *Chem. Sci.*, 2019, **10**, 10209–10230.

5 C. Liu, J. Wang, J. Wan and C. Yu, *Coord. Chem. Rev.*, 2021, **432**, 213743.

6 C. Mellot-Draznieks, C. Serre, S. Surblé, N. Audebrand and G. Férey, *J. Am. Chem. Soc.*, 2005, **127**, 16273–16278.

7 S. Surblé, C. Serre, C. Mellot-Draznieks, F. Millange and G. Férey, *Chem. Commun.*, 2006, 284–286.

8 T. Chalati, P. Horcajada, R. Gref, P. Couvreur and C. Serre, *J. Mater. Chem.*, 2011, **21**, 2220–2227.

9 W.-T. Xu, L. Ma, F. Ke, F.-M. Peng, G.-S. Xu, Y.-H. Shen, J.-F. Zhu, L.-G. Qiu and Y.-P. Yuan, *Dalton Trans.*, 2014, **43**, 3792–3798.

10 K.-Y. A. Lin, H.-A. Chang and C.-J. Hsu, *RSC Adv.*, 2015, **5**, 32520–32530.

11 J. Wang, J. Wan, Y. Ma, Y. Wang, M. Pu and Z. Guan, *RSC Adv.*, 2016, **6**, 112502–112511.

12 X. Liao, F. Wang, F. Wang, Y. Cai, Y. Yao, B.-T. Teng, Q. Hao and L. Shuxiang, *Appl. Catal., B*, 2019, **259**, 118064.

13 E. Bagherzadeh, S. M. Zebarjad and H. R. M. Hosseini, *Eur. J. Inorg. Chem.*, 2018, 1909–1915.

14 C. Mellot-Draznieks, C. Serre, S. Surblé, N. Audebrand and G. Férey, CCDC 644016, *Experimental Crystal Structure Determination*, 2007.

15 C. Serre, C. Mellot-Draznieks, S. Surblé, N. Audebrand, Y. Filinchuk and G. Férey, CCDC 644019, *Experimental Crystal Structure Determination*, 2007.

16 Y. Li, Y.-X. Zhou, X. Ma and H.-L. Jiang, *Chem. Commun.*, 2016, **52**, 4199–4202.

17 H. Fu, X.-X. Song, L. Wu, C. Zhao, P. Wang and C.-C. Wang, *Mater. Res. Bull.*, 2020, **125**, 110806.

18 V. P. Viswanathan, S. V. Mathew, D. P. Dubal, N. N. Adarsh and S. Mathew, *ChemistrySelect*, 2020, **5**, 7534–7542.

19 H. Wu, M.-D. Ma, W.-Z. Gai, H. Yang, J.-G. Zhou, Z. Cheng, P. Xu and Z.-Y. Deng, *Environ. Sci. Pollut. Res.*, 2018, **25**, 27196–27202.

20 S. Xue, J. Li, L. Zhou, J. Gao, G. Liu, L. Ma, Y. He and Y. Jiang, *J. Agric. Food Chem.*, 2019, **67**, 13518–13525.

21 W. Wu, J. Wang, T. Zhang, S. Jiang, X. Ma, G. Zhang, X. Zhang, X. Chen and B. Li, *J. Mater. Chem. C*, 2019, **7**, 5451–5460.

22 Stoe & Cie, *X-Red and X-AREA*, Darmstadt, Germany, 2009.

23 G. M. Sheldrick, *Acta Crystallogr., Sect. A: Found. Crystallogr.*, 2015, **71**, 3–8.

24 G. M. Sheldrick, *Acta Crystallogr., Sect. C: Struct. Chem.*, 2015, **71**, 3–8.

25 A. L. Spek, *Acta Crystallogr., Sect. C: Struct. Chem.*, 2015, **71**, 9–18.

26 C. F. Macrae, I. Sovago, S. J. Cottrell, P. T. A. Galek, P. McCabe, E. Pidcock, M. Platings, G. P. Shields, J. S. Stevens, M. Towler and P. A. Wood, *J. Appl. Crystallogr.*, 2020, **53**, 226–235.

27 L. Wang, Y. Zhang, X. Li, Y. Xie, J. He, J. Yu and Y. Song, *Sci. Rep.*, 2015, **5**, 14341.

28 J. Amaro-Gahete, R. Klee, D. Esquivel, J. R. Ruiz, C. Jiménez-Sanchidrián and F. J. Romero-Salguero, *Ultrason. Sonochem.*, 2019, **50**, 59–66.

29 H. Jeong and J. Lee, *Eur. J. Inorg. Chem.*, 2019, 4597–4600.

30 K.-Y. Andrew Lin and F.-K. Hsu, *RSC Adv.*, 2015, **5**, 50790–50800.

31 P. Gao, R. Liu, H. Huang, X. Jia and H. Pan, *RSC Adv.*, 2016, **6**, 94699–94705.

32 P. Hirschle, C. Hirschle, K. Böll, M. Döblinger, M. Höhn, J. M. Tuffnell, C. W. Ashling, D. A. Keen, T. D. Bennett, J. O. Rädler, E. Wagner, M. Peller, U. Lächelt and S. Wuttke, *Chem. Mater.*, 2020, **32**, 2253–2263.